Development of Spheroidized Graphite Cast Iron Material for Spent Fuel Transport and Storage Cask and Investigation of its Mechanical Properties

O. Tsumura, S. Shimizu, M. Murata, Y. Tanaka, M. Maruoka, I. Sato and K. Suzuki

The Japan Steel Works, Ltd., Muroran Plant
4 Chatsu-machi, Muroran, Hokkaido, 051, Japan

1. INTRODUCTION

The DCI to be used in manufacturing spent fuel transport and storage casks will be extremely thick (500mm). As a part of the study program for evaluating economic feasibility as well as for establishing standards for DCI casks, the manufacturing of large-model casks and collection of data were started by each material manufacturer (a round robin test). It is well known that, as thickness increases, the graphite structure in spheroidized graphite cast iron is deformed, and graphite chunks are more likely to be produced. There exists, therefore, the necessity to elucidate what factors control these characteristics.

For this study, we manufactured a 40ton (large and thick) casting to simulate an actual-size cask. After performing nondestructive examination, we cut the casting into sections. We conducted various mechanical tests at the center of the wall thickness of these sections to investigate DCI's material properties.

2. TEST METHODS

2.1 Shape of Test Model

We manufactured a test model with a wall thickness of 500 mm (based on the wall thickness required in actual casks). The test model was designed to be a cylinder with a circular bottom. This would allow simulating as close as possible the solidification condition of the casting, which is postulated to be the most critical technical control factor when manufacturing spent fuel transport and storage casks. Fig.1 shows the shape of the test model that was manufactured for the study. Both the height and outside diameter of the test model were 2000mm. This is somewhat smaller than an actual cask.

2.2 Casting Procedure and Test Items

2.2.1 Casting procedure

The mold used was chilled on its entire face, which was backed by self-hardening sand. In addition, cooling by mist was applied on the inside surface of the casting. This enabled control of the eutectic solidification time, a determining factor in the improvement of ductility. Fig.2 shows the elongation and corresponding eutectic solidification times that were obtained in previous studies (Iwabuchi et al. 1987). It is clear from the figure that the degree of elongation sharply improves if the eutectic solidification time is two hours or less.

The contents of C and Si, the most important chemical elements, were determined from the minimum and maximum wall thicknesses of a casting. Impurity elements such as Mn, Ca, Ce, As and Sb were controlled to avoid the formation of chunky graphite or graphite flake. Raw materials were first melted and desulfurized in a basic arc furnace, and the molten metal then was cast by spheroidizing

and inoculation through commercial chargings processing agents. Based on economical considerations, we adopted the riser-free casting process. The chemical composition, inoculation and graphitization, pouring temperature and cooling were subjected to stringent control. Fig.3 shows the casting process flow.

In addition, we measured cooling temperatures from pouring with thermocouples inserted into the surface layer, 1/4T, and center to evaluate the eutectic solidification time and cooling rate. The casting thus prepared was subjected to annealing at 900°c to obtain the ferrite base structure of more than 90%. We determined the precise shape of the chilling block through computer solidification simulation.

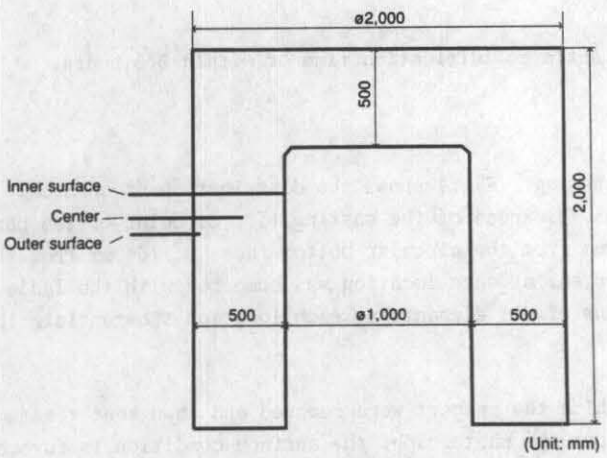

Fig. 1 Configuration and locations of thermocouples for model cask

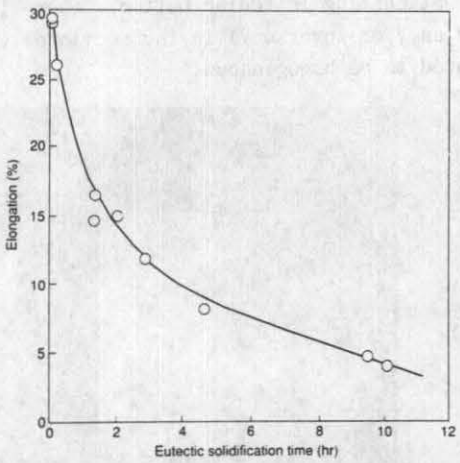

Fig. 2 Relationship between elongation and eutectic solidification time

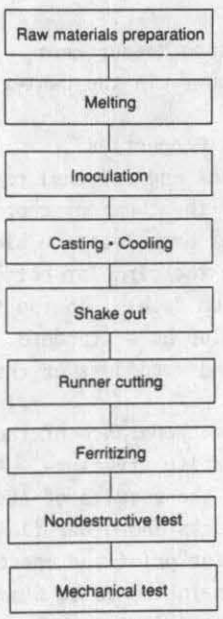

Fig. 3 Manufacturing sequence of model cask

Photo 1 Model cask

2.2.2 Test items

(1) Internal properties and structures

After machining the longitudinal section in the center of the casting, we conducted the liquid penetrant test, sulfur print test, and macro-etching test using 10% nital. Next, we sampled specimens from locations along the sectional thickness and performed chemical analysis and microstructure examinations. In addition, we measured the nodularity (in accordance with the standard established by the Japanese Society of Casting Engineers) (Tanimura 1968), ferrite area ratio, and graphite distribution density.

(2) Mechanical tests

We prepared JIS No.4 tensile test pieces and JIS No.4 test pieces with a 2mm V-notch for the Charpy impact test from the specimens sampled from the locations along the sectional thickness.

(3) Fracture toughness test

We measured static fracture toughness KIc in accordance with the unloading compliance method by using the displacement control-type tester (Iwadate 1983). The piece used for the test was an IT-CT type having a groove 12.5% in depth, 0.25mm in tip radius and 45 degrees in angle on both sides.

3. TEST RESULTS

3.1 Temperature Measurement

The cooling curve in the center retains the eutectic solidification time of within 2.5 hours.

3.2 Material Properties

3.2.1 External and internal properties

Table 1 shows the chemical composition of the casting. Fig.4 shows the distribution of chemical composition at each location along the sectional thickness of the casting (TT: circular bottom part, T: 560mm from the circular bottom face, M: 1250mm from the circular bottom face, B: 1640mm from the circular bottom face). In the figure, the C content at each location was compared with the ladle analysis C value as a standard. Small variations of all elements at each location substantiate the homogeneity and soundness of the casting.

Photo 1 is the appearance of the casting from which the runners were removed and then heat treated to obtain the ferrite structure. As can be seen from the photograph, the surface condition is favorable. Photo 2 shows the results of the liquid penetrant test. The longitudinal section is free of shrinkage, cracks and other flaw indications, thus demonstrating good internal soundness. Photo 3 shows the sulfur print and macro-etching structure of one side of the longitudinal section. Although there is dross in the 40 to 50mm range on the top side at casting (circular bottom), there is neither microstructural deficiency nor macro-segregation (such as V or inverse-V) in the sectional thickness or top-bottom direction. Thereby, the casting has proved to be homogeneous.

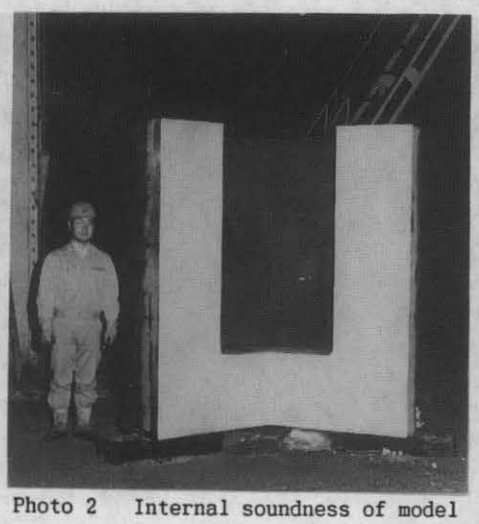

Photo 2 Internal soundness of model cask (liquid penetrant test)

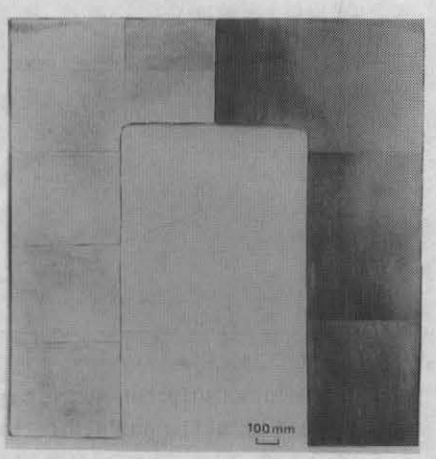

Photo 3 Sulfur print and macro-structure of model cask

Table 1 Chemical composition of model cask (wt.%)

C	Si	Mn	P	S	Mg
3.65	1.80	0.12	0.031	0.003	0.08

3.2.2 Microstructure

Photo. 4 shows the microstructures at locations T and B along the sectional thickness. Fig.5 shows measurements of the nodularity, graphite particle size, and ferrite content ratio. The nodularity decreases from both the inner and outer surface layers towards the center, and it tends to be slightly lower on the T-side than on the B-side. However, the nodularity at the center of the TT location, where it is expected to be of the lowest figure, is more than 75%. A favorable spheroidized structure is obtained, as supported by the microstructure in Photo 4.

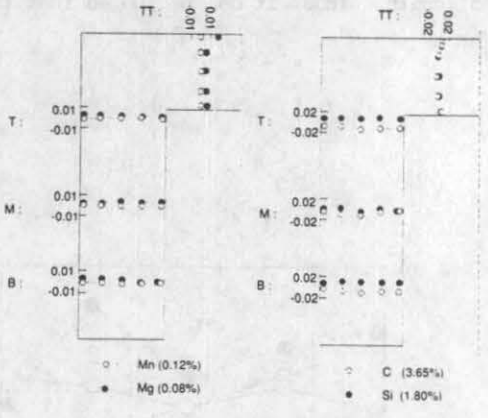

Fig. 4 Distribution of chemical composition of model cask

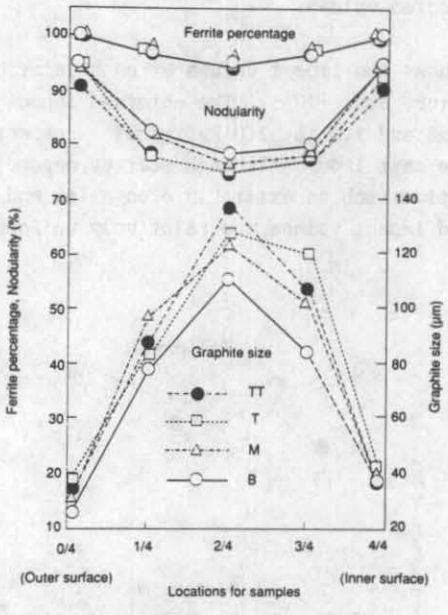

Fig. 5 Graphite size, nodularity and ferrite percentage of model cask

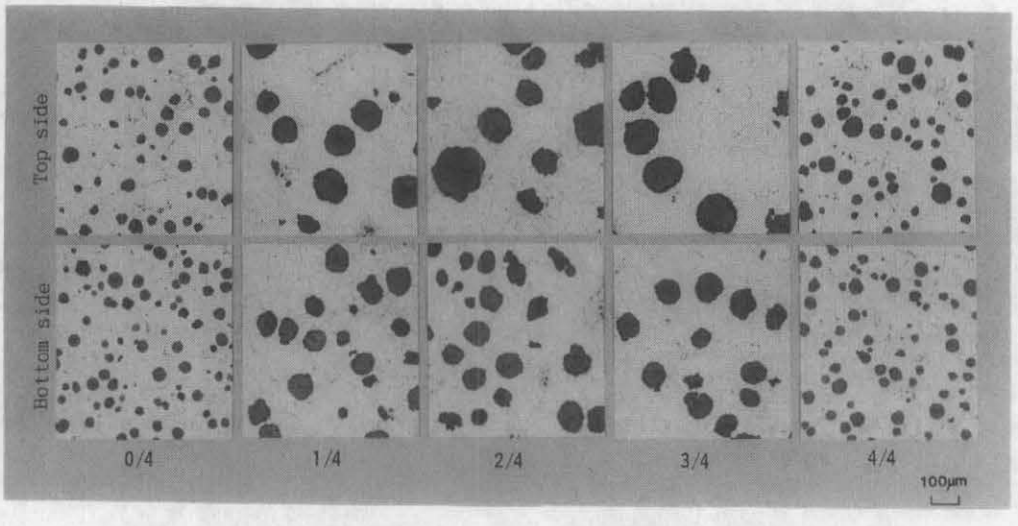

Photo 4 Microstructure at various portions of model cask

On the other hand, the graphite particle size on the surface layer is 35μm to 40μm, but it coarsens to 100 μm to 138 μm in the center part. The ferrite content ratio has a similar tendency to decrease to some extent towards the center part, whereas the amount of pearlite increases. However, there is more than 95% ferrite content ratio in the center, showing almost no difference through the T-B direction. Thus, the form of graphite is favorable at any location with high ferrite content ratio.

3.2.3 Mechanical properties

3.2.3.1 Tensile and impact properties

Fig.6 shows the tensile strength, yield strength and elongation obtained at room temperature. Yield strength is almost constant through the sectional thickness at all locations (about 22 kgf/mm²). The behavior of tensile strength and elongation is almost the same. Both the tensile strength and elongation decrease from the surface layer of the sectional thickness towards the inner part. They are lowest in the center and produce lower values on the T-side than on the B-side. However, the lowest tensile strength and elongation are more than 32 kgf/mm² and 12%, respectively, both surpassing the expected values.

Fig.7 shows the impact values at each location along the sectional thickness tested at room temperature and -40°C. The obtained impact values at room temperature and at -40°C are 2.0 to 3.0 kgf.m/cm² and 1.0 to 2.0 kgf.m/cm² , respectively. These are good impact values for spheroidized graphite cast iron. Although scatter depending on the sampling location exists, there is no distinct correlation such as exists in elongation and tensile strength. Thus, it can be judged that the obtained impact values are relatively uniform.

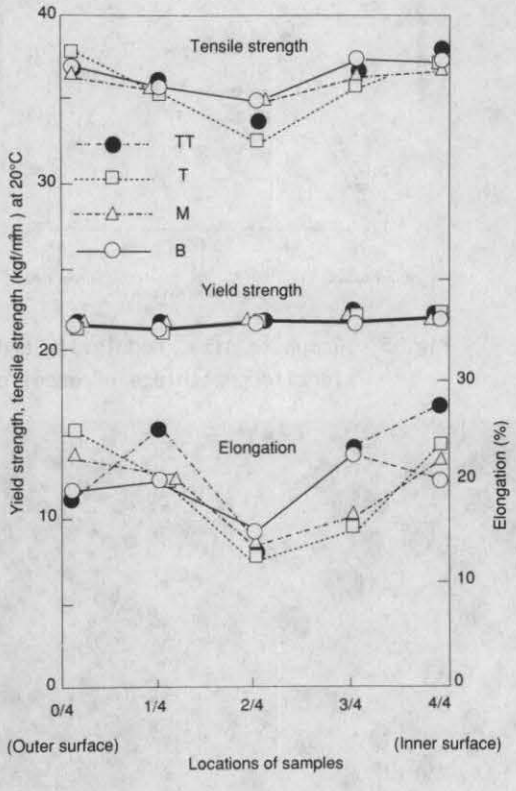

Fig. 6 Tensile properties of model cask

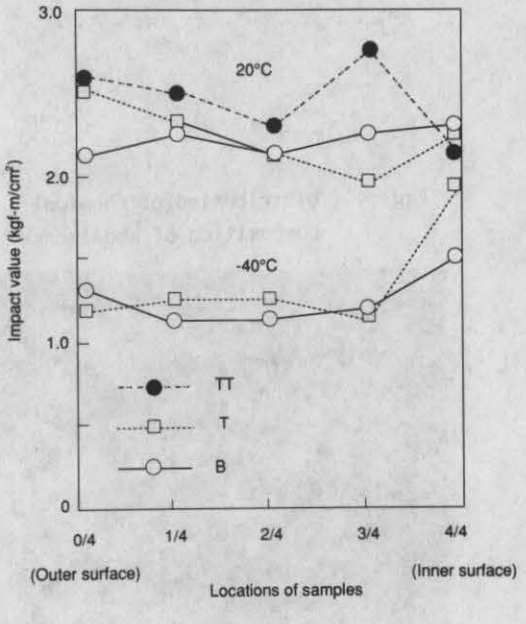

Fig. 7 Impact values of model cask

3.2.3.2 Fracture toughness

We measured fracture toughness, KId(J) and KIc(J), at room temperature and -40°C at each location along the sectional thickness at the M location of the casting. Fig.8 shows the results. KIc at both temperatures is nearly uniform along the sectional thickness. However, KIc at the outer surface layer is slightly lower in the the same manner as for the impact value. This can be ascribed to smallness of graphite particle size. KId also shows equal values along the sectional thickness. The 2/4 T test specimen shows the lowest KId in the room temperature test.

4. STUDIES OF METALLURGICAL PROPERTIES AND MECHANICAL PROPERTIES

As the tests and examinations of the model cask have made clear, it is difficult to obtain homogeneous properties throughout the wall thickness of a thick-walled spheroidized graphite cast iron. In particular, scatters of graphite particle size are large. Therefore, we prepared test materials of different graphite particle sizes to study the relationship between graphite particle size and mechanical properties.

Fig.9 shows the relationship between elongation and graphite particle size with a parameter of nodularity. Elongation is shown to increase as the nodularity increases. Moreover, the degree of elongation is influenced by graphite particle size. The relationship between elongation and graphite particle size shown in Fig.9 reveals that elongation increases as the particle size increases, but it decreases as the particle size becomes larger than 75μm.

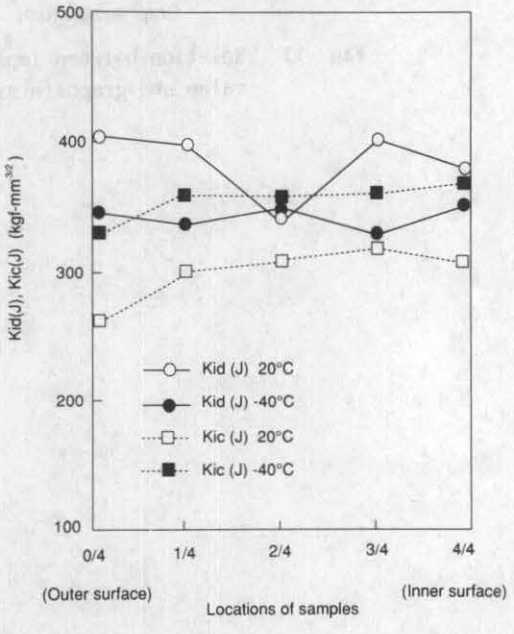

Fig. 8 Fracture toughness of model cask

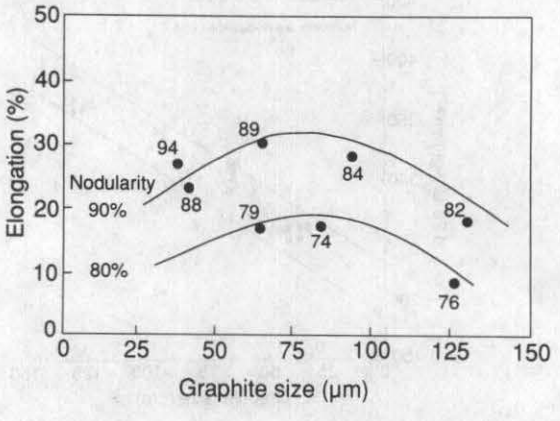

Fig. 9 Relation between elongation and graphite size

Next, we will consider the relationships between graphite shape/size and impact value/fracture toughness. Figs. 10 and 11 show the relationship between impact value and nodularity and between impact value and graphite particle size, respectively. It is difficult to establish a distinct correlation between impact value and graphite particle size, since the obtained range of impact values is narrow. However, we can observe a tendency that increase in graphite particle size serves to improve impact strength. On the other hand, the dependence of the impact value upon the nodularity is small, there being only small scattering when the nodularity exceeds 70%.

Fig.12 shows the relationship between graphite particle size and fracture toughness. From the figure, it is clear that fracture toughness in the test range that we applied this time does not depend on the nodularity. Instead, it is more dependent on the particle size. Fracture toughness improves as the graphite particle size becomes coarser. Since fracture toughness is controlled by the distance over which cracks connect to each other from graphite to graphite, it thus becomes dependent on the graphite particle size as long as there is no difference in the graphite area ratio and the ferrite base structure.

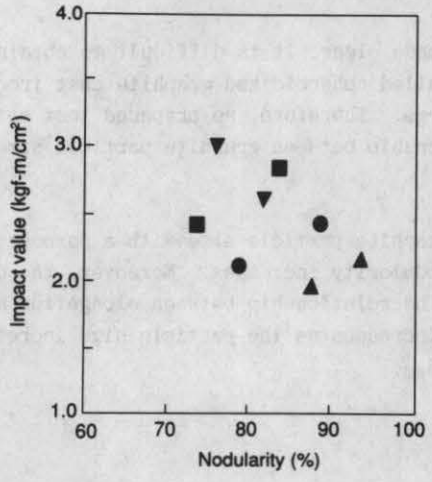

Fig. 10 Relation between impact value and nodularity

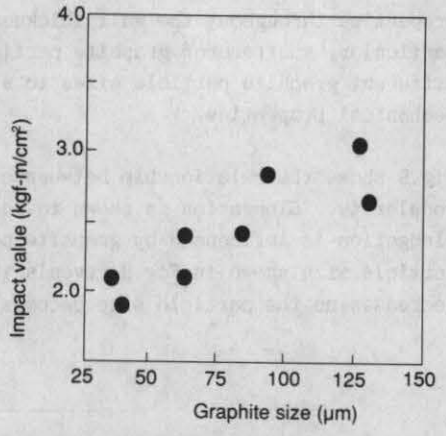

Fig. 11 Relation between impact value and graphite size

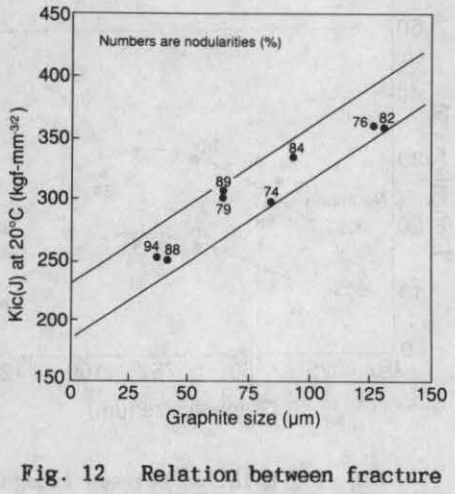

Fig. 12 Relation between fracture toughness and graphite size

5. CONCLUSIONS

We manufactured a 500mm thick ferrite base, spheroidized graphite cast iron cylindrical casting with a circular bottom (2000mm outside diameter and 2000mm height) for trial purpose. We then investigated the basic quality and performance by sampling specimens from various locations of the product. The results of the study can be summarized as follows.

(1) Although there were some casting wrinkles, the overall surface of the casting was found to be good, without blowholes and other defects. In addition, the internal properties were sound, free of casting defects, macro-segregation and variations in chemical composition.

(2) The nodularity tended to decline at the center of the interior where solidification occurred slowly. However, the nodularity was more than 75%, and no abnormal graphite was observed. Similarly, the ferrite area ratio had a tendency to decrease at the center, but it remained at more than 95%.

(3) Yield strength and impact value were almost constant through the sectional thickness. The yield strength and impact value at room temperature were about 22 kgf/mm^2 and 2.0 to 3.0 kgf.m/cm^2, respectively. On the other hand, tensile strength and elongation varied from part to part, and they tended to be lower at the center and towards the direction of the T-side. However, we obtained the tensile strength and elongation of more than 32 kfg/mm^2 and 12%, respectively, at all parts.

(4) Variation in dynamic as well as static fracture toughness along the sectional thickness was relatively small, the values being nearly uniform. Moreover, KIc and KId exceeded 300 kgf.mm$^{-3/2}$ at the test temperature of -40°c.

(5) The degree of elongation tended to improve with increases in the nodularity. Elongation was also dependent on graphite particle size. The best elongation was obtained with the graphite particle size of about 75 μm, and it declined above and below the 75μm level.

(6) Both the impact value and fracture toughness had little dependence on nodularity in the test range. They increased almost linearly, however, with increase in graphite particle size.

References

Iwabuchi, Y., Narita, H. and Ichinomiya, Y., Castings, 59 (1987) 3, p.153.

Iwadate, T., Tanaka, Y., Ono, S., and Tsukada, H., Tetsu to Hagane, 69 (1983) 2, p.308.

Tanimura, Casting,40 (1968) 3, P.148.